Int. J. Electrochem. Sci., 15 **(2020)** 2528 – 2538, doi: 10.20964/2020.03.48

International Journal of
ELECTROCHEMICAL
SCIENCE
www.electrochemsci.org

The Performance of a Novel PdFe/B-N-G Catalys for Ethanol Electro-oxidation in Alkaline Medium

Wenhui Geng, Mengmeng Zheng, Dan Chen, Xianwen Wang, Zekai Zhang, Yishan Lin, Dongqin Cai, Huiqin Li, Guobo Huang, Yanxian Jin[*], *Binbin Yu*[*]

School of Pharmaceutical and Material Engineering, Taizhou University, Taizhou 318000 , China
[*]E-mail: snowflakej@163.com

Received: 22 October 2019 / *Accepted:* 30 December 2019 / *Published:* 10 February 2020

Palladium catalyst (Pd) are made attention to application in alcohol fuel cells due to unique performance, as well as the resource abundance and low cost, but the catalyst performance and stability of the catalysts are still not satisfied. In this article, the novel PdFe/B-N-G catalysts with the double element alloying and dual-doping for ethanol electro-oxidation are successfully prepared and determined by XRD, TEM and XPS. TEM results reveal a relatively uniform and high dispersion of Pd particles is observed on PdFe/B-N-G catalyst. The XPS analysis indicates that Pd(0) contents of the PdFe/B-N-G catalyst are increased on account of the B, N-doping effect. Being explored as the catalyst to the ethanol oxidation reactions, the PdFe/B-N-G catalysts exhibit the better electrocatalytic activity with higher current densities and catalyst stability compared to those of PdFe/G and Pd/B-N-G, which can be attributed to the synergistic effect of the enhanced PdFe alloying and the B, N-doping, that can produce more activity sites dispersing on the surface of graphene. Thus, the novel PdFe/B-N-G catalysts can be the potential alternate in alcohol fuel cells.

Keywords: Ethanol Electro-oxidation; PdFe catalyst; B, N doping; Alcohol Fuel Cells.

1. INTRODUCTION

As a kind of effective clean energy technology to suitable for energy demand, fuel cells are attracted extensive attentions all over the world. Many kinds of low temperature fuel cells, especially direct alcohol fuel cells such as direct methanol fuel cells (DMFCs) and direct ethanol fuel cells (DEFCs), have made great progress in recent years [1-3]. In compared to methanol system, ethanol system display the higher specific energy density and more environmentally friendly, which results in the rapidly development of direct ethanol fuel cells (DEFCs) [4-6].

Some previous reports have shown that the Pd catalyst exhibits much better electro-catalytic activity and stronger resistance to poison than those of the Pt catalyst in alkaline systems in DEFCs. Moreover, Pd metal is more resource abundant and much lower cost than Pt (1/3 of the Pt cost) [7]. Therefore, various Pd catalysts have aroused increasing interest in electrocatalytic activity of ethanol oxidation in alkaline media. However, there is still a problem that Pd will be slowly poisoned by the adsorption by-product such as the CH_3CO during ethanol electrooxidation, thus leading to the sharp decline of the electrocatalytic activity and poor stability [6-8]. Hence, it is essential and meaningful to find effective ways to improve the electrocatalytic activity and stability and even reduce the ratio of Pd metal from the catalyst, such as the doping a second or third non-noble metal into Pd catalysts (Co, Ni, Cu, Fe and so on) [9-13].

Graphene is widely used as a support electrode material in fuel cells owing to its good conductivity and high surface area. It is generally known that heteroatom doping especially doping with N or B atom can enhance the electrochemical performance of graphene [14]. In recent years, a number of studies reported that dual-doping like B, N [15] and N, P-doped [16] graphene has exhibited better performance for oxygen reduction reaction than single-atom doped graphene, which probably be ascribed to the synergistic effect of B-N co-doping that may produce different activity sites on the graphene surface [8,15,16]. Therefore, this can be the effective way to enhance the electrochemical properties and stability of the catalysts. So far, as we know, there is few studies on B-N doped graphene (B-N-G) as the support of Pd alloy catalysts for the ethanol electro-oxidation reactions.

In this paper, the novel PdFe/B-N-G catalysts with the double element alloying and dual-atom doping for ethanol electrooxidation are successfully prepared, which have been characterized by XRD, TEM and XPS. Moreover, the catalytic activity and stability of PdFe/B-N-G catalysts towards ethanol electro-oxidation have been investigated compared with Pd/G, PdFe/G and Pd/B-N-G.

2. EXPERIMENTAL PART

2.1. Materials

Graphite (99.95%), ferric chloride hexahydrate ($FeCl_3$. $6H_2O$) were purchased by Aladdin, Aqueous ammonia (AR, >25%), H_2SO_4 (98%) were purchased by Zhejiang HanNuo chemical technology Co, potassium boron hydride (KBH_4), H_3BO_3 (99%), and palladium chloride ($PdCl_2$) were purchased from Shanghai Chemical Reagent Co.

2.2. Catalyst preparation

Firstly, the Graphene oxide (GO) material was prepared by Hummers method from graphite powder [17]. Then, the B-doped graphene (B-G) was synthesized as follows: 0.2 g of GO were added to 20 ml of distilled water, then H_3BO_3 solution (1.546 g boric acid dissolving with 30 mL of distilled water) was put into the mixture with ultrasonically stirring to form a uniform suspension. The suspension was transferred into a Teflon-lined stainless steel autoclave and maintained at 135℃ for 6 h. Then the

product was filtered and calcinated at 400℃ under a Ar atmosphere at a heating rate of 5 ℃/min. Finally, the sample was filtered, washed by water and acetone for several times, and then dried at 60℃ for 12h.

Next, the B-N co-doped graphene (B-N-G) was synthesized as follows: the as-prepared B-G sample (0.2g) was put into 50 mL concentrated ammonia solutions, and then the mixture was transferred to the hydrothermal reactor and heated at 190℃ for 6 h. After cooled and filtered, the product was washed with distilled water for several times and dried under vacuum at 60 ℃ for 12h.

The novel catalyst Palladium supported boron-nitrogen doped graphene (Pd/B-N-G) was prepared by potassium boron hydrogenation reduction method [19]. 80 mg B-N-G carrier was put into 30 mL distilled water, and then 2.46 mL 0.05 mol/L $PdCl_2$ solutions and 0.033 g $FeCl_3.6H_2O$ was added and ultrasonicated for 10 min. The obtained slurry was transferred to a three-neck bottle and heated to 50℃ for 4 h. Then 316 mg KBH_4 was dissolved in 120 mL distilled water and slowly dropped KBH_4 solution. After the reaction, the product was then filtered, dried at vacuo at 50℃ for 12h, and the catalyst PdFe/B-N-G was successfully obtained.

The reference substances Palladium supported graphene (Pd/G) was synthesized by the similar method of potassium boron hydrogenation reduction method without the B-N codoping or the $FeCl_3.6H_2O$. The Palladium/iron supported graphene (PdFe/G) and the Palladium supported boron-nitrogen doped graphene (Pd/B-N-G) were synthesized by the similar method without the B-N codoping and without $FeCl_3.6H_2O$, respectively.

2.2. Catalyst characterization.

X-ray diffraction (XRD) tests were measured in Bruker AXS D8 Advance X-ray Diffractometer with a CuKα source (λ = 0.15406 nm) operating at 40 kV voltages and 40 mA current. The patterns were collected in a 2θ range from 5 to 90° at a step of 0.0167°. X-ray photoelectron spectroscopy (XPS) measurements were performed using Escalab 250Xi photoelectron spectroscopy with an Al Ka target. Transmission electron microscope (TEM) images were carried out with JEOL-2010 microscope (200 kV, 103 mA).

2.3. Electrochemical measurement.

The electrode was prepared as follows: a certain amount of ethanol, 5 wt% Nafifion solution and 5 mg of catalyst powders were mixed under sonication. 5 uL of ink-like suspension was dropped onto the glassy carbon electrode (GCE, 0.1256 cm^{-2}) with 4mm diameter, and dried at room temperature, thus it was used as working electrode. The final catalyst loading was 0.0875 mg. cm^{-2}.

The electrochemical performances of various samples were carried out in a conventional three-electrode system at CHI730d electrochemical workstation using the as-prepared electrode as the working electrode, a Pt foil as the auxiliary electrode and the saturated calomel electrode (SCE) electrode as the reference electrode in nitrogen-saturated 1 $mol \cdot L^{-1}$ KOH electrolyte with a scan rate of 20 mV/s. The Cyclic voltammograms were tested in 1 M KOH+ 1M CH_3CH_2OH solution for Pd/G, Pd/B-N-G, PdFe/G and PdFe/B-N-G electrodes with the scan rate of 20 mV/s. The Chronoamperometric were tested for

Pd/C, Pd/B-N-G, PdFe/G and PdFe/B-N-G electrodes in 1 M KOH+ 1M CH_3CH_2OH solution at 0.4 V vs. SCE.

3. RESULTS AND DISCUSSION

3.1. Physicochemical characterization

Figure 1 depicts XRD diagrams for Pd/G, Pd/B-N-G, PdFe/G and PdFe/B-N-G. As shown, all four catalysts have diffraction peaks C (002) at about 26° in 2θ, indicating that the graphene oxide was successfully reduced to form graphene [18].

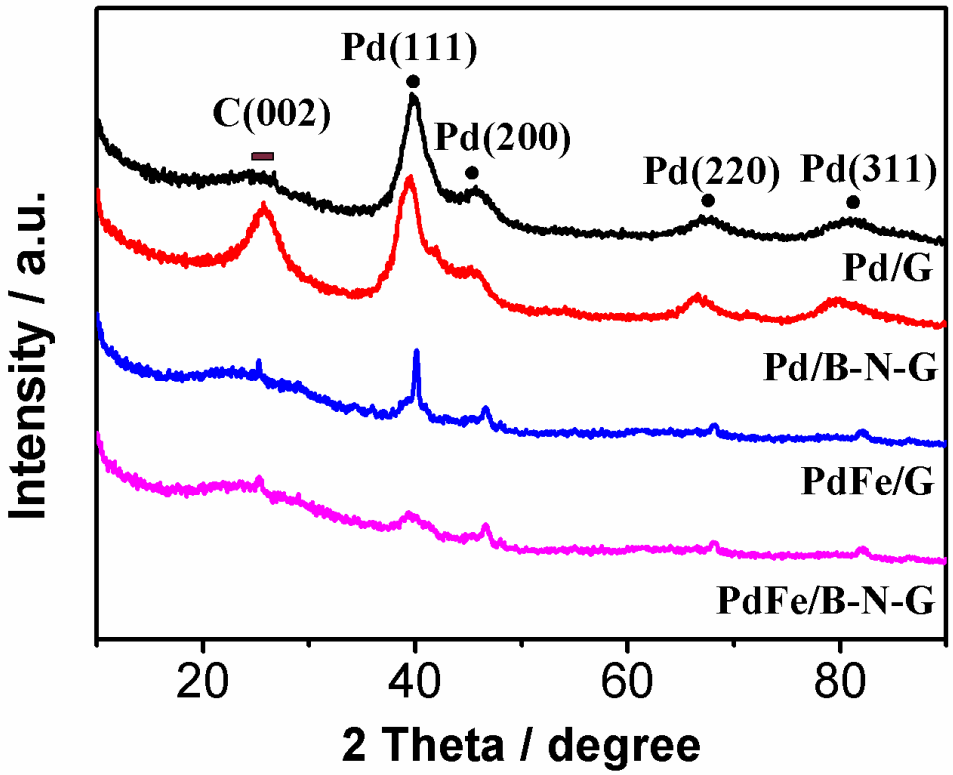

Figure 1. XRD patterns of Pd/G, Pd/B-N-G, PdFe/G and PdFe/B-N-G Samples

Moreover, the four peaks at 39.8°, 45.6°, 67.6° and 81.1° all appear on the four catalysts, which correspond to Pd (111), (200), (220) and (311) lattice planes of Pd crystal. These results indicate that Pd has been successfully loaded onto the B-N-G carrier. In addition, in contrast to Pd/G and Pd/B-N-G, the diffraction peaks of PdFe/G and PdFe/B-N-G move slightly towards the high diffraction angle, and no Fe diffraction peak are identified. It can be explained that Fe metal successfully enters the Pd lattice to form a PdFe alloy.

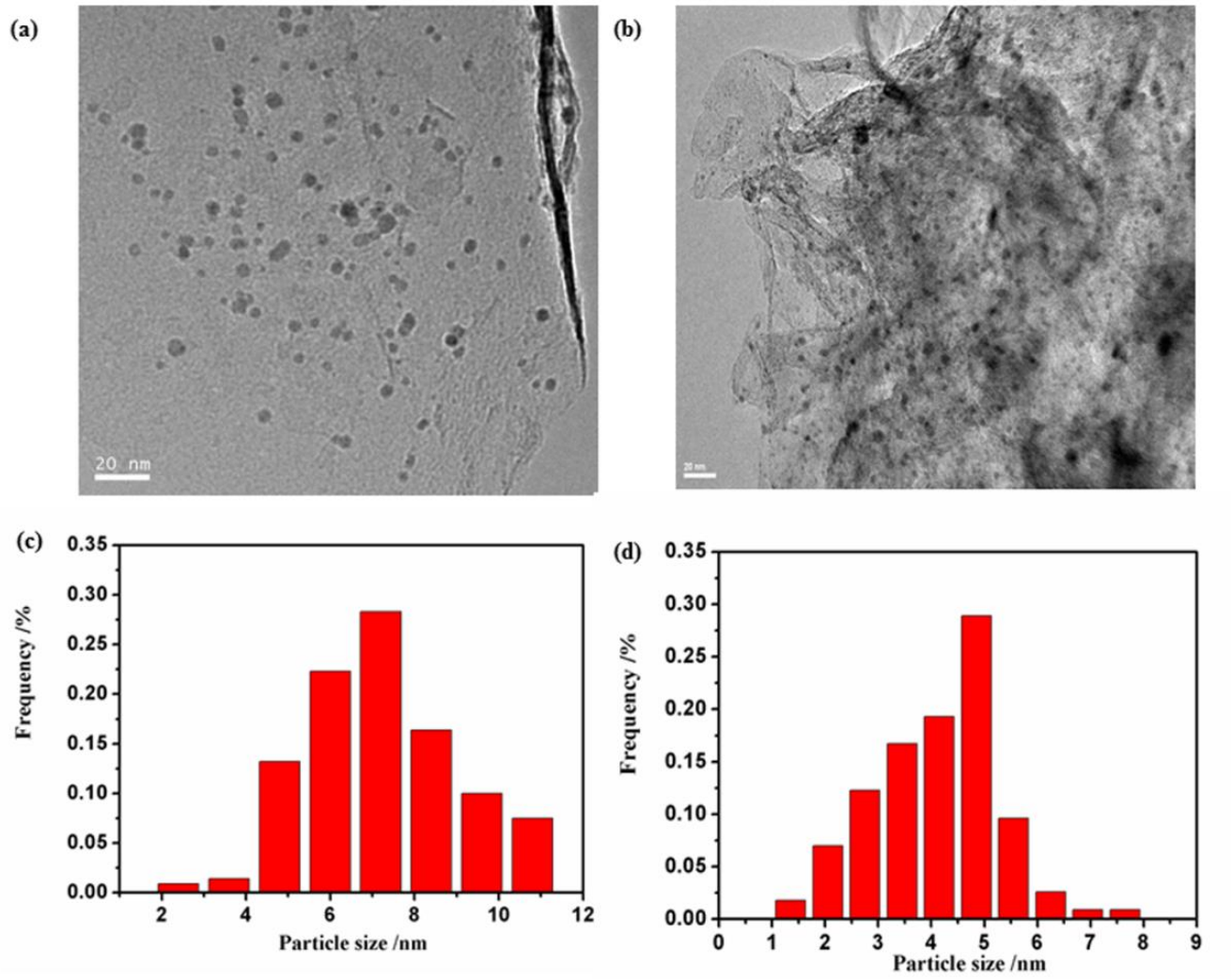

Figure 2. TEM images of PdFe/G (a), PdFe/B-N-G (b) and the particle size distribution of PdFe/G (c), and PdFe/B-N-G (d)

Figure 2a and 2b represent TEM images of PdFe/G and PdFe/B-N-G catalysts, respectively. It can be observed that the graphene presents nanosheet structure with some folds, and some Pd spherical particles are dispersed on the graphene carrier. In comparison, a relatively uniform and high dispersion of Pd particles is observed on PdFe/B-N-G catalyst (Figure. 2b). Moreover, Pd catalyst particle size distribution of PdFe/G and PdFe/B-N-G catalysts are further analyzed, as shown in Figure 2c and 2d. Pd particles of PdFe/G catalyst range from 2 to 12 nm with average particle size of 7.6 nm. In contrast, Pd particles on PdFe/B-N-G catalyst have much narrower size distribution between 1 to 8 nm with the average particle size of 4.7 nm, which illustrates the more fine and homogeneous distribution of Pd particles.

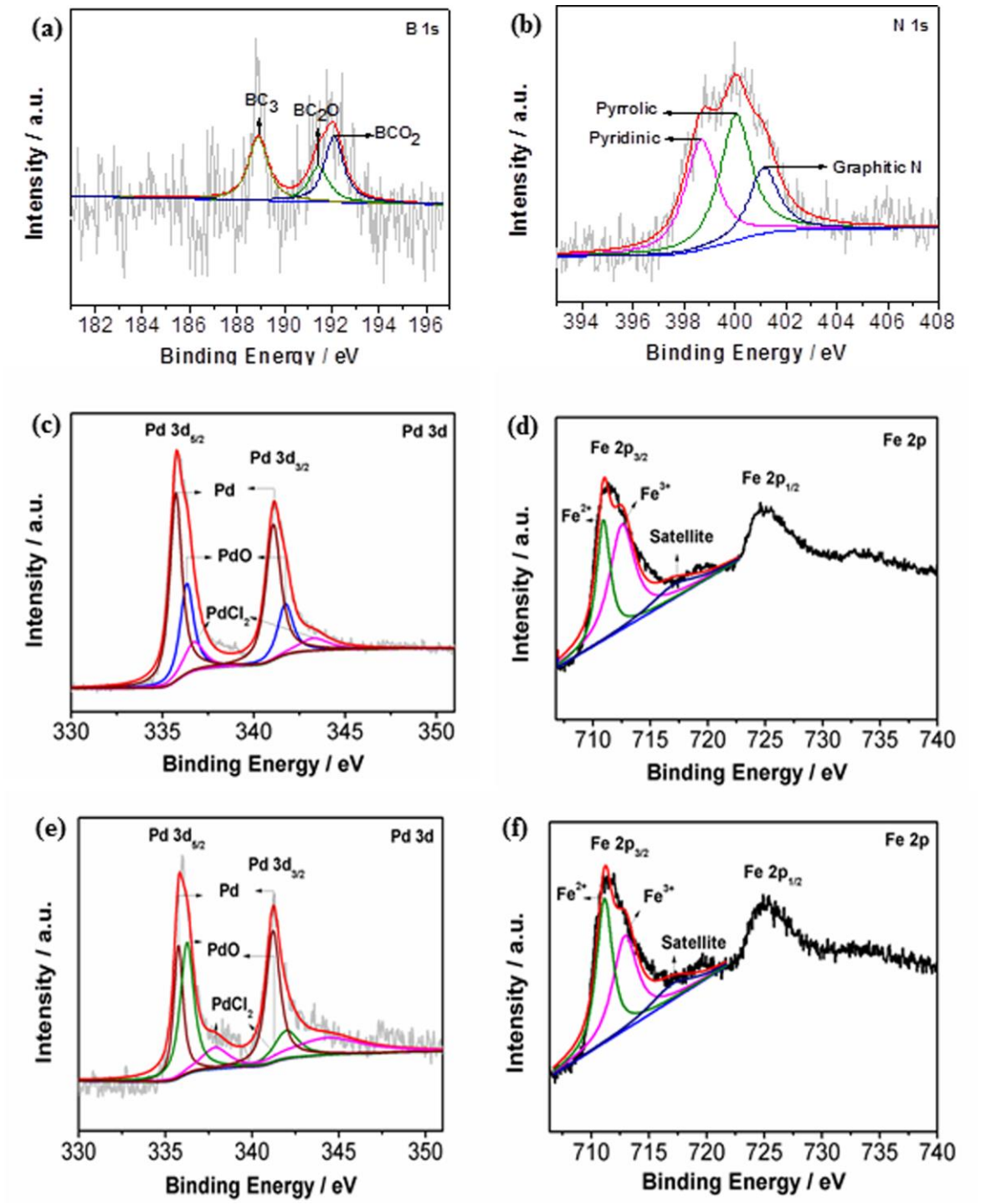

Figure 3. a–d) XPS spectra PdFe/B-N-G. High-resolution spectra of a) B 1s, b) N 1s, c) Pd 3d and d) Fe 2p. e–f) XPS spectra PdFe/G. High-resolution spectra of e) Pd 3d and f) Fe 2p.

In our case, we can also conclude that the defective sites introduced by boron and nitrogen codoping onto graphene, which are beneficial to anchor metal nanoparticles, and then promote the high dispertion of Pd nanoparticles.

Moreover, the XPS data were further applied in the analysis of the detail chemical composition and electronic structure of the PdFe/B-N-G catalyst and PdFe/G catalyst.

According to the curve fitting of the B 1s and N 1s spectra, it can be observed that B and N

elements bond to graphene in the form of chemical bonds, respectively, manifesting that both of N and B have been successfully doped with the graphene (Figure 3a and 3b). As for the Pd 3d spectra of PdFe/B-N-G and PdFe/G catalysts (Figure 3c and 3e), it can be observed that all of the six peaks appear on the PdFe/B-N-G and PdFe/G catalysts, in which the characteristic peaks of Pd located at 335.67 eV and 341.17 eV, the peaks of PdO at 336.27 eV and 341.79 eV, the peaks of Pd^{2+} located at 336.76 eV and 343.2 eV, respectively [8, 19]. Compared to those of PdFe/G catalyst, Pd contents increase while the Pd^{2+} contents decrease on the PdFe/B-N-G , which can be attributed to the B and N dual doping produce the collective electronic effect on Pd, that produce more metallic Pd [8]. Similarly, as we see the Fe 2p spectra of PdFe/B-N-G and PdFe/G catalysts (Figure 3d and 3f), the peak of 710.8 eV, 712.92 eV and 717.63 eV can be explained the characteristic peaks of Fe^{2+}, Fe^{3+} and Fe, respectively. In contrast, the signal peak intensities of Fe^{2+} and Fe^{3+} of PdFe/B-N-G samples are higher than those of PdFe/G samples. These results indicate the co-doping of B and N elements can promote the alloying of Pd and Fe, thus may improving the catalyst performance.

3.2. Electrochemical characterization

The cyclic voltammograms of Pd/G, Pd/B-N-G, PdFe/G and PdFe/B-N-G were evaluated in 1 mol/L KOH solution at a scan rate of 20 mv/s and shown in Figure 4. All of the four catalysts exhibit the pair of redox characteristic peaks, in which the oxidation peak located at 1.3V and the reduction peak located at 0.6V.

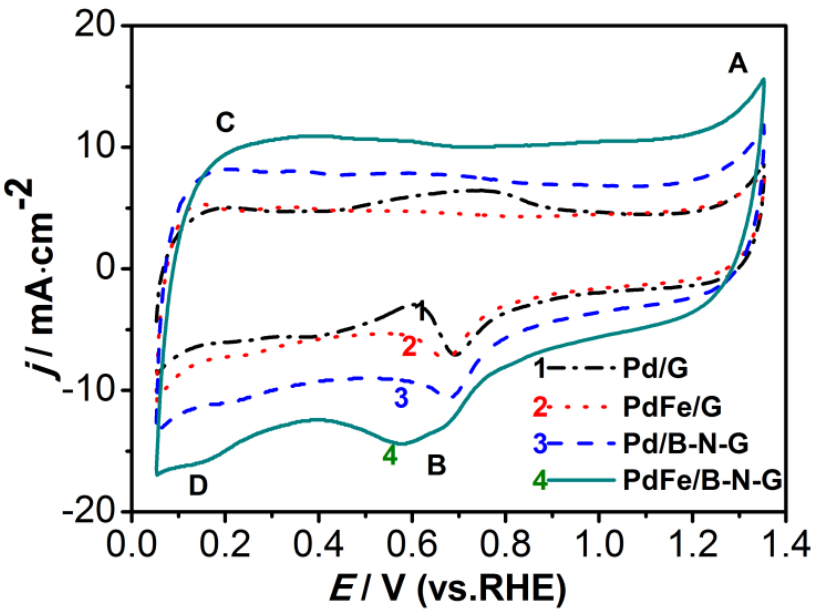

Figure 4. Cyclic voltammogram curve of Pd/G, PdFe/G, Pd/B-N-G and PdFe/B-N-G electrodes in nitrogen-saturated 1 mol·L^{-1} KOH electrolyte with a scan rate of 20 mV/s

The redox peaks can be ascribed to the oxidation (A) and reduction (B) of Pd oxide. Meanwhile, it can be observed that the pair of weak redox peaks at 0.2V/0.1V, which can be ascribed to the absorption

(C) and desorption (D) of hydrogen [20]. In the cathodic scans, the PdFe/G, PdFe/B-N-G both show more negative shifting of the cathodic potentials compared with the Pd/G, indicating the electronic structure on the surface of Pd-Fe is changed after alloying with Fe. It is worth mentioning that the more electron back-donation from Fe sites to Pd sites can be attributed to the electronic modification of Pd structure due to the B, N- doping on the graphene. According to the reduced peak area, the catalyst of the load PdFe alloy has a large reduced peak area, and the electrochemical surface area of PdFe/B-N-G is the largest, which can result in the better electrochemical activity of the oxygen reduction reaction.

Figure 5 shows the electrocatalytic activities of Pd/G, Pd/B-N-G, PdFe/G and PdFe/B-N-G electrodes in 1mol/L KOH and 1mol/L CH_3CH_2OH solution at a scan rate of 20 mV/s by the cyclic voltammogram tests. And the current density of the oxidation peak can show the activity of the catalyst to some extent. As we see, all of the four electrodes exhibit the similar oxidation peaks that are present at around 0.8V, which attribute to the oxidation of ethanol. In contrast, the B, N co-doped graphene has the higher current density than that of graphene without doping, which indicates the synergistic effect of B-N co-doping that may produce different activity sites on the graphene surface, thus improving the catalyst activity. In addition, the current density of the load PdFe alloy is higher than that of the load Pd, so the load PdFe alloy is conducive to the further improvement of catalyst activity. Of course, it can be expected that the PdFe/B-N-G catalyst with the double metals alloying and dual-doping reveal the best catalyst activity. The Table 1 shows the comparison of corresponding Pd catalysts with similar two metals alloying for ethanol oxidation in literatures. Though the research results cannot be compared one to one owing to the different experiment condition, we can also conclude that the novel catalyst PdFe/B-N-G exhibits the excellent electrocatalystic activity in contrast to the other Pd catalysts, which can be attributed to the synergistic effect of the enhanced PdFe alloying and the B, N-doping, that can produce more activity sites dispersing on the surface of graphene.

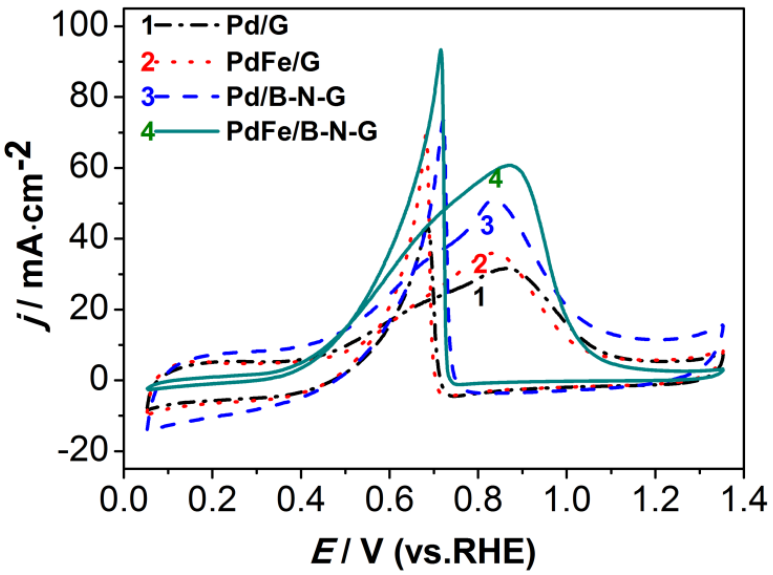

Figure 5. Cyclic voltammograms in 1 M KOH+ 1M CH_3CH_2OH solution for Pd/G, Pd/B-N-G, PdFe/G and PdFe/B-N-G electrodes. Scan rate: 20 mV/s

Table 1. The electrocatalytic data on different Pd catalysts for ethanol electro-oxidation in alkaline medium

Pd catalyst in the literature	Electrocatalytic activity
Pd/C [20]	2.8 mA cm-$^{-2}$ in 0.5M ethanol in 1M KOH
$Pd_{86}Sn_{14}$/C [20]	8 mA cm^{-2} in 0.5M ethanol in 1M KOH
Pd-Co/RGO [21]	500 mA mg^{-1} in 1M ethanol in 1M KOH at 25 mV/s
Pd_1Fe_1 porous carbon nanofibers [7]	250 mA mg-1 in 1M ethanol in 1M KOH at 50mV/s
Pd_2Fe_1 porous carbon nanofibers [7]	1500 mA mg-1 in 1M ethanol in 1M KOH at 50mV/s
Pd porous carbon nanofibers [7]	800 mA mg-1 in 1M ethanol in 1M KOH at 50mV/s
PdFe/B-N-G (in this work)	60 mA cm^{-2} or about 700 mA mg^{-1} in 1M ethanol in 1M KOH at 20 mV/s

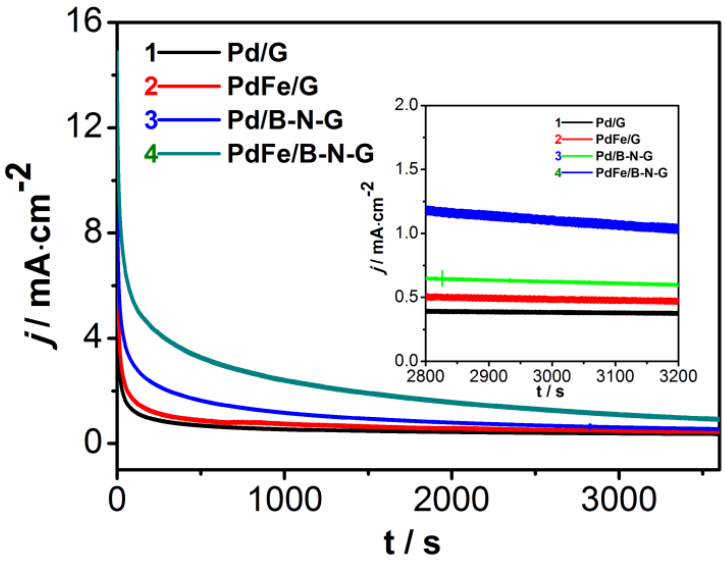

Figure 6. Chronoamperometric curves of Pd/C, Pd/B-N-G, PdFe/G and PdFe/B-N-G electrodes in 1 M KOH+ 1M CH_3CH_2OH solution at 0.4 V vs.SCE

In order to further investigate the stability of the PdFe/B-N-G catalyst, the chronoamperometric curves of the four catalysts are measured in 1 M KOH+ 1M CH_3CH_2OH solution at 0.4 V vs. SCE and shown in Figure 6. At the beginning, all of the current intensities show the sharp decline as the time increased, which probably can be attributed to the by-product toxic substances that are produced and accumulated on the surface of the catalyst during the ethanol oxidation process. With the time goes by, the Pd/Fe-B-N-G catalyst exhibits the highest current intensity in the four catalysts. In particular, the Pd/Fe-B-N-G catalyst shows 3 times higher current density than Pd/G after 3200s, indicating the strongest resistance to poison to the toxic by-product (CO*) due to the synergistic effect of B-N co-

doping and PdFe alloying. Thus, the novel palladium-based materials based on dual metals alloying and dual elements doping can be the potential candidate for ethanol oxidation in alkaline medium.

4. CONCLUSIONS

In the summary, the novel PdFe/B-N-G catalysts with the double element alloying and dual doping, and another three reference catalysts are successfully prepared. The detail chemical composition and electronic structure of the catalysts are also determined by XRD, TEM and XPS analysis. The cyclic voltammograms and chronoamperometric curves both show that the PdFe/B-N-G catalyst reveal the better electrochemical activity and stronger resistance to poison than those of another three catalysts, which can attribute to the synergistic effect of B-N co-doping and PdFe alloying. Thus, the novel PdFe/B-N-G catalysts can be the potential alternate in alcohol fuel cells.

ACKNOWLEDGMENTS
This work was supported by Natural Science Foundation of Zhejiang Province, China (Nos. LTY20B030002), National Natural Science Foundation of China (Nos.21671146,Nos. 21403150), Zhejiang Provincial College Students' science and technology innovation project (2017R430016), College Students' science and technology innovation project of Taizhou City() and College Students' science and technology innovation project of Taizhou University.

References

1. D. Chen, Z.S. He, S.E. Pei, L.A. Huang, H.B. Shao, Y.X. Jin and J.M. Wang, *J. Alloy. Compounds*, 785 (2019) 781.
2. R. Arukula, M. Vinothkannan, A.R. Kim and D.J. Yoo, *J. Alloy. Compounds*, 771 (2019) 477.
3. M.M. Tian, S. Shi, Y.L. Shen and H.M. Yin, *Electrochim. Acta*, 293 (2019) 390.
4. P. Wu, Y. Huang, L. Zhou, Y. Wang, Y. Bu and J. Yao, *Electrochim. Acta*, 152 (2015) 68.
5. J. Ye, D.Y. Kim, S.W. Kang, K.W. Choi, S.W. Han and O.O. Park, *Nanoscale*, 6 (2014) 4182.
6. Q. Dong, Y. Zhao, X. Han, Y. Wang, M. Liu and Y. Li, *Int. J. Hydrogen Energy*, 39 (2014) 14669.
7. M. Wei, L. Zhang , D. Luo, L.X. Ding, S.Q. Wang and H.H. Wang, *Electrochim. Acta*, 289 (2018) 311.
8. Y.X. Jin, D.M. Han, W.P. Jia, G.B. Huang, F. Li, X.Y. Chen, R.R. Li, M.M. Zheng and W.Y. Gao, *J. Electrochem. Society*, 164 (2017) 638.
9. Y. Wang, Q. He, J. Guo, J. Wang, Z. Luo, T.D. Shen, K. Ding, A. Khasanov, S. Wei and Z. Guo, *Appl. Mater. Interfaces*, 7 (2015) 23920.
10. Z. Zhang, C. Zhang, J. Sun, T. Kou, Q. Bai, Y. Wang and Y. Ding, *J. Mater. Chem*. A, 1 (2013) 3620.
11. A.L. Wang, X.J. He, X.F. Lu, H. Xu, Y.X. Tong and G.R. Li, *Angew. Chem. Int. Ed*., 54 (2015) 3669.
12. R.N. Singh, A. Singh, Carbon, 47 (2009) 271.
13. P. Mukherjee, P.S. Roy, K. Mandal, D. Bhattacharjee, S. Dasgupta and S.K. Bhattacharya, *Electrochim. Acta*, 154 (2015) 447.
14. C.H. Choi, M.W. Chung, H.C. Kwon, S.H. Park and S.I. Woo, *J. Mater. Chem*. A, 1 (2013) 3694.
15. J. Liang, Y. Jiao, M. Jaroniec and S.Z. Qiao, *Angew. Chem. Int*. Ed., 51 (2012) 11496.

16. Y. Zheng, Y. Jiao, L. Ge, M. Jaroniec and S.Z. Qiao, *Angew. Chem. Int*. Ed., 125 (2013) 3192.
17. S.Y. Zhao, J. Liu, C.X. Li, W.B. Ji, M.M Yang, H. Huang, Y. Liu and Z.H. Kang, *Appl. Mater. Interfaces,* 6 (2014) 2229.
18. K.N. Kudin, B. Ozbas, H.C. Schniepp, R.K. Prud' homme, I.A. Aksay and R. Car, *Nano Letter*, 8 (2008) 36.
19. Y.X. Jin, J. Zhao, F. Li, W.P. Jia, D.X. Liang, H. Chen, R.R. Li, J.J. Hu, J.M. Ni, T.Q. Wu and D.P. Zhong, *Electrochim. Acta*, 220 (2016) 83.
20. W.X. Du, K.E. Mackenzie, D.F. Milano, N.A. Deskins, D. Su, and X.W. Teng, *ACS Catalysis*, 2 (2012) 287.
21. Y. Wang, Y. Zhao, J. Yin, M.C. Liu, Q. Dong, Y.Q. Su, *Int. J. hydrogen Energy*, 39 (2014) 1325.